Carbon emission reduction requires attention to the contribution of natural gas use: Combustion and leakage

Haoyuan Chen[1, 5], Tao Song[1,5]*, Xiaodong Chen[2], Yinghong Wang[1], Mengtian Cheng[1], Kai Wang[1], Fuxin Liu[4], Baoxian Liu[3], Guiqian Tang[1, 5]*, Yuesi Wang[1, 5]

Correspondence to Guiqian Tang (tgq@dq.cern.ac.cn) Tao Song (st@dq.cern.ac.cn)

1. Key Laboratory of Atmospheric Environment and Extreme Meteorology, Institute of Atmospheric Physics, Chinese Academy of Sciences, Beijing, China

2. Beijing Aozuo Ecological Instrument Co., Ltd., Beijing 100080, China

3. Beijing Key Laboratory of Airborne Particulate Matter Monitoring Technology, Beijing Municipal Environmental Monitoring Center, Beijing, 100048, China

4. Anhui University of Science and Technology, Anhui 232001, China

5. University of Chinese Academy of Sciences, Beijing 100049, China

Abstract: Natural gas will continue to replace coal in the process of global energy structure reform, but its leakage potential can delay the realization of global carbon neutrality. To quantify its impact, we established a carbon dioxide (CO_2) and methane (CH_4) flux detection platform on the 220-m platform of the Institute of Atmospheric Physics, Chinese Academy of Sciences, located in northwestern Beijing. The observation results indicated that the daily mean CO_2 and CH_4 fluxes were 12.21 ± 1.75 $\mu mol \cdot m^{-2} \cdot s^{-1}$ and 95.54 ± 18.92 $nmol \cdot m^{-2} \cdot s^{-1}$, respectively. The fluxes were significantly correlated with natural gas consumption, indicating that natural gas has become a common source of CH_4 and CO_2, the combustion of which releases CO_2, while its leakage processes emit CH_4. Vehicle-based identification demonstrated that CH_4 can escape at the production, storage and use stages of natural gas. Based on natural gas consumption data, the upper limit of the calculated natural gas leakage rate in Beijing reached $1.12 \% \pm 0.22 \%$, indicating that the contribution of CH_4 to climate change could reach 23 % of that of CO_2 on a 20-year scale. Natural gas leakage was estimated to delay the time for China to achieve carbon neutrality by at least almost four years.

KEY WORDS:

CO_2 flux, CH_4 flux, Eddy covariance, Natural gas leakage, Climate forcing, Carbon neutrality

1. INTRODUCTION

In 2015, the 1.5 °C temperature control target was proposed in the Paris Agreement to reduce

the occurrence of extreme weather events(Seneviratne et al., 2018). To achieve this goal, it is necessary to actively promote the low-carbon development transformation of the economic system, especially energy transformation. In this process, natural gas plays an important role, and typical countries have indicated a trend of coal reduction and gas increase during energy structure adjustment over the past century. It is expected that global natural gas consumption will continue to increase by 2035.

Natural gas is commonly referred to as a clean alternative to coal, but its main component is methane, with a global warming potential (GWP) that is 29.8 times greater than that of carbon dioxide at the hundred-year scale(Environmental-Protection-Agency, 2024). If 3.4 % of methane leaks into the atmosphere before natural gas combustion, the advantages of natural gas over coal will become negligible(Kemfert et al., 2022). Recent studies have suggested that the average loss rate of natural gas in cities worldwide ranges from 3.3 % to 4.7 %(Sargent et al., 2021). According to statistics from the International Energy Agency (www.iea.org) in 2020, methane leakage in the global oil and gas industry reached 72 million tons and amounted to 6 billion tons of carbon dioxide equivalent (CO_2e) within 20 years. Therefore, it is unclear whether natural gas can become a bridging material for energy transformation.

One important prerequisite is to determine the contribution of natural gas leakage during coal-to-gas conversion to urban methane(CH_4) emissions and its climate effects. At present, conventional CH_4 monitoring methods include ground, aviation, and satellite monitoring methods. Ground monitoring aims to detect the atmospheric CH_4 concentration through the installation of sensors and monitoring stations at fixed locations or on vehicles(Wunch et al., 2016). Notably, monitoring equipment is often installed near potential emission sources, with high detection accuracy but generally a limited spatial range. The aviation monitoring method can be employed to identify large-scale CH_4 emissions through measurement techniques such as drones or aircraft but cannot be used to achieve long-term monitoring(Duren et al., 2019; Frankenberg et al., 2016; Sherwin et al., 2024). Satellite methods can compensate for the shortcomings of the former two methods(Chen et al., 2022; Cusworth et al., 2018; Shen et al., 2023), which exhibit interference from clouds and require significant labor and financial investments.

The eddy covariance method, which is based on tall towers, enables long-term monitoring of methane emissions, thus facilitating the identification of methane sources in specific areas. However,

61   it should be noted that this method has certain limitations during urban flux measurements at higher

62   altitudes, as larger air volumes in the measurement system may lead to a significant imbalance

63   between the observed vertical turbulence exchange and surface net flux compared with those at

64   typical measurement heights. However, this deficiency should be considered in conjunction with

65   the advantages of urban tower measurements because cities typically correspond to deeper rough

66   sublayers that can extend to 2–5 times the average building height(Barlow, 2014). Therefore,

67   increasing the measurement altitude can help characterize the turbulent exchange between this layer

68   and the inertial sublayer.

69   Developing countries are the main driving force behind the continuous growth in global energy

70   demand. As Beijing is the capital of the world's largest developing country and the first city within

71   China to complete the coal-to-gas conversion process, clarifying the natural gas leakage process in

72   Beijing can provide guidance for energy transformation in developing countries regionally and even

73   globally. In this study, three aspects related to natural gas were investigated as follows. First, the

74   fluxes of CH_4 and CO_2 were observed simultaneously via the eddy covariance method, which was

75   used to investigate the impact of the coal-to-gas policy on CO_2 and CH_4 in Beijing, including the

76   magnitude of CO_2 emission and the common effects on the sources of both. Second, with navigation

77   experiments, the natural gas leakage process in Beijing has been confirmed, and the emission levels

78   of natural gas at different stages have been further roughly estimated, which provides certain

79   effective insights for the control of natural gas leakage in Beijing. Third, we discuss climate forcing

80   caused by natural gas leakage while considering the CO_2 flux as a basis, calculate the natural gas

81   leakage rate with statistical data, and estimate the impact of natural gas leakage on China's carbon

82   peak and carbon neutrality in conjunction with existing reports.

83

84   **2. METHODS**

85   **2.1 Instrument setup for eddy covariance measurement**

86   The measurements were conducted at a 325-m high meteorological tower in northwestern

87   Beijing, with a closed-path observation system installed on a platform at a height of 220 m, which

88   included a dual laser gas analyzer (QC-TILDAS-DUAL, Aerodyne Research Inc., USA), three-

89   dimensional ultrasonic anemometer (Gill Instruments, Ltd., Lymington, Hampshire, UK), vacuum

90   pump (XDS35i, BOC Edwards, UK), data collector (CR6, Campbell Scientific Inc., USA), and

91   other accessories. In the dual laser gas analyzer, tunable infrared laser direct absorption spectroscopy

92   (TILDAS) technology is used to detect the most significant fingerprint transition frequencies of

93   molecules within the mid-infrared wavelength range. The analyzer has an optical path of up to 76

94   m and can measure H_2O, CO_2 and CH_4 simultaneously. Similar instruments have been applied to

95   observe outdoor ecosystems(Zöll et al., 2016). Under the action of a vacuum pump, the air sample

96   enters the instrument room at a flow rate of 2 lpm through a polytetrafluoroethylene sampling tube

97   with a length of 3 m and an inner diameter of 3 mm (Figure S1). Instrument calibration includes

98   zero-point and range calibration processes. High-purity nitrogen gas (>99.999%) was used for zero-

99   point calibration at 1-hour intervals. In this process, the corresponding solenoid valve was opened,

100   which was automatically controlled by TDLWintel software, and range calibration was performed

101   at the factory. In addition, before the experiment, we calibrated the gas analyzer using CO_2 (401

102   ppm) and CH_4 (2190 ppb) standard gases. We found that the measured and standard gas

103   concentrations differed by less than 1%, indicating satisfactory instrument performance. Therefore,

104   we did not perform range calibration later. The instrument was placed in an insulated box equipped

105   with air conditioning to ensure normal operation of the laser. Both instruments were operated at a

106   sampling frequency of 10 Hz. The data collector and high-frequency instrument were timed

107   according to the network and global positioning system (GPS), respectively, to maintain

108   synchronization. To minimize the twisting effect of the flux tower on the incoming air, a three-

109   dimensional ultrasonic anemometer was installed at the end of a 1.5-m long support arm facing

110   southeast China in summer. This measurement lasted from June 11 to September 7, 2022, during

111   which the nitrogen cylinder was replaced, and the instrument was debugged on June 18 and 19.

112   From July 12 to 26, the experiment was stopped due to failure of the tower power supply.

113   **2.2 Flux data processing**

114   The flux data processing operation in this study is based on the eddy covariance technique via

115   EddyPro software (version 6.2.1, Li COR, Inc.; Lincoln, Nebraska, USA). An average flux

116   calculation period of 30 minutes was selected(Lee, 2004). Before calculating half-hourly fluxes,

117   spike detection and data rejection algorithms were applied like follows as described by Vickers et

118   al., (1997): Take a moving window with a width equal to 1/6 of the averaging period (typically 5

119   minutes) and calculate the mean and standard deviation of the time series within the window. Define

120   outliers as any data points deviating from the mean by n times the standard deviation (initial n =

3.5). Replace the identified outliers with linearly interpolated values from adjacent points. Consecutive outliers ≤ 3 are treated as a single outlier; consecutive outliers ≥ 4 are considered local trends and excluded from outlier classification. Iteratively increase n by 0.1 per cycle until no outliers are detected or 20 iterations are reached. Advance the window by half its width (step size) and repeat outlier detection/removal for the next window. Continue this process until all outliers are processed within the averaging period. If outliers exceed 1 % of the total data points in any averaging period, discard that entire period.

The double rotation method proposed by Kaimal et al., (1994) was employed for tilt correction. The delay time caused by the spatial separation of gas analyzers and three-dimensional ultrasonic anemometers (as well as the injection pipeline of closed-path systems) was corrected via the maximum covariance method(Fan et al., 2012). Webb, Pearman, and Leuning (WPL) correction was not applied here(Webb et al., 2007) because the instrument room was in a state of constant temperature and pressure that converted the real-time concentration into a dry volume mixing ratio, and the longer pipeline of the closed-path system avoided the influence of temperature fluctuations. The limitations of eddy covariance systems can lead to frequency loss in flux observations. Factors such as a limited average period and linear detrending can cause low-frequency loss, whereas instrument separation, path averaging, insufficient high-frequency responses, and pipeline attenuation can cause high-frequency loss. The method proposed by Moncrieff et al., (1996) was employed for frequency response correction. After the above correction of the flux data, in this paper, the 0-1-2 quality labeling scheme proposed by Mauder and Foken(Mauder et al., 2004) was adopted for data quality control purposes. Notably, a value of 0 represents data with the best quality, a value of 1 represents data with good quality, and a value of 2 represents data with poor quality. In this study, flux data marked as 2 were excluded from the subsequent analysis. In addition, the flux source area was evaluated via the method of Kljun et al., (2004) (Text. S1), and the flux source area covered most of the urban area of Beijing and reflected the average emission characteristics of urban Beijing (Figure S2).

2.3 Spectral analysis

High-frequency signal loss can occur in closed-path systems. To determine the response capability of the closed-path system to high-frequency turbulence signals, we analyzed the observed gas exchange signals through the turbulence power spectrum. The selected time ranges from 12:00

151 to 16:00 every day during the observation period, with a total of 8 and a half hours of data. The data

152 were integrated and averaged, and the data curve was then compared with the ideal slope in the

153 inertia subarea (Figure S3). $Co(wT)$ followed the theoretical $f_n^{-4/3}$ (where f_n denotes the normalized

154 frequency) in the inertial subregion. In contrast, the slopes of $Co(wCO_2)$ and $Co(wCH_4)$ were

155 slightly greater than -4/3, indicating that there was high-frequency loss in the flux observations of

156 the closed-loop system(Kaimal et al., 1972). Through high-frequency correction, the calculation

157 results indicated that the CO_2 and CH_4 fluxes were 7.73 % and 6.85 % greater, respectively, than

158 those before correction.

159 **2.4 Mobile CH_4 and CO_2 observations**

160   Vehicle-based experiments were conducted in the urban area of Beijing in the winter of 2023

161 and the summer of 2024, and the specific deployment of the mobile observation station is shown in

162 Figure S1. Notably, the car was equipped with a CO_2/CH_4 spectrometer (Los Gatos Research, Inc.,

163 USA), a laptop for data viewing, and a mobile power supply (Figure S4). Zero-point calibration of

164 the instrument was performed once pure nitrogen was used before the mobile experiment began.

165 Standard gases of methane and carbon dioxide were introduced to calibrate the instrument

166 simultaneously, and we found that the concentration of the instrument matched well with the

167 standard gas. Since we focused more on the enhancement in concentration rather than itself, we did

168 not calibrate it again afterward. The sampling port was located approximately 20 cm from the roof,

169 and ambient air was collected through a PTFE tube with a length of 2 m and an inner diameter of 3

170 mm. Before the particulate matter entered the instrument, it was removed using a filter head. The

171 IMET sounding instrument (International Met Systems, USA) is installed on the roof, with a

172 sampling frequency that is consistent with that of the other instruments, i.e., 1 s, real-time

173 concentration information of different latitudes and longitudes is obtained at a resolution of seconds

174 through the corresponding time between the GPS and the instrument; for example, if the GPS

175 sampling time delay is 3 s, the latitude and longitude coordinates are reassigned to the CH_4 reading

176 observed three seconds prior. Our observation sites include petrochemical plants located in

177 southwestern Beijing, natural gas storage tanks and landfills in the northeastern part, and power

178 plants with the highest natural gas usage in the southeastern part.

179 **3. RESULTS**

3.1 Diurnal variation in the flux

A positive or negative flux reflects the vertical exchange direction of trace gases in the urban canopy, which is positive upward and negative downward. (The uncertainty analysis is described in the Text. S2 and Figure S5, respectively) Overall, both CO_2 and CH_4 fluxes are positive on a daily scale, indicating that cities are the source of both gases. The diurnal CO_2 flux ranged from 6.05 to 19.66 $\mu mol \cdot m^{-2} \cdot s^{-1}$ with an average of 12.21 ± 1.75 $\mu mol \cdot m^{-2} \cdot s^{-1}$(Figure 1a), which was generally lower than the summer observations by Cheng et al., (2018) and Liu et al., (2012) at 200 m and 140 m at this tower, respectively(Table.S1), a smaller deviation suggests that CO_2 may be dominated by a more stable source than before. We also obtained observation results at 140 m in summer from 2009–2017 (Liu et al., 2020). The flux in 2022 significantly decreased compared with previous levels (Figure S6), which reflects the transformation of Beijing's energy structure. The coal-to-gas policy implemented by Beijing these years led to a gradual decrease in the proportion of coal in primary energy consumption, with a steady increase in the proportion of natural gas in total consumption (Figure S7), the use of natural gas results in much less coal CO_2 than coal, generating the same amount of heat; moreover, Beijing has increased the amount of electricity flow from other provinces in recent years (Figure S7), which has further driven a decrease in the annual average concentration of $PM_{2.5}$, dropping to 30.5 $\mu g \cdot m^{-3}$ by 2024. In fact, previous studies have reported a high correlation between $PM_{2.5}$ and CO_2 fluxes. For example, Donateo et al., (2019) found that the seasonal and daily variations in the particle number flux in southern Italian suburbs are largely determined by both transportation activities and household heating. Liu et al., (2020) confirmed that the CO_2 flux can explain 64 % of the interannual variation in the $PM_{2.5}$ concentration by fitting the correlation between the annual average $PM_{2.5}$ and CO_2 fluxes in Beijing from 2009 to 2017. Therefore, controlling CO_2 emissions can also greatly control the concentration level of $PM_{2.5}$, thereby achieving the dual effects of mitigating climate change and improving air quality. In terms of its diurnal variation, it did not follow a typical bimodal pattern but rather remained high after reaching the first peak at 8:00, with a lower level at night, reflecting high anthropogenic carbon emissions during the day, such as those resulting from transportation and energy generation activities. The diurnal pattern of the CH_4 flux was similar to the observation results of Giolo et al., (2012) and Helfer et al., (2016) (Figure 1b), reflecting an increase in emissions during the day. The CH_4 flux began to increase gradually from 04:00 to around 08:30, and then remained stable until

210 after 10:30, when it began to rise rapidly again, reaching its daily peak of approximately 157.1 nmol

211 m^{-2} s^{-1} around 11:30. After 17:30, it slowly declined. Its diurnal variation pattern showed some

212 differences compared to CO_2 flux, which increased beginning at 03:30 to around 08:30 similar to

213 CH_4 flux. However, the peak for CO_2 flux occurred around 13:30, then slowly decreased and

214 decreased rapidly after 18:30, Assuming that the average CH_4 flux at midnight (00:00 to 06:00) can

215 be employed as the baseline for nighttime emissions, it accounted for 58% of the daily average flux.

216 The CH_4 flux demonstrated a pronounced diurnal pattern, indicating a significant daily variation in

217 the background source in the source area.
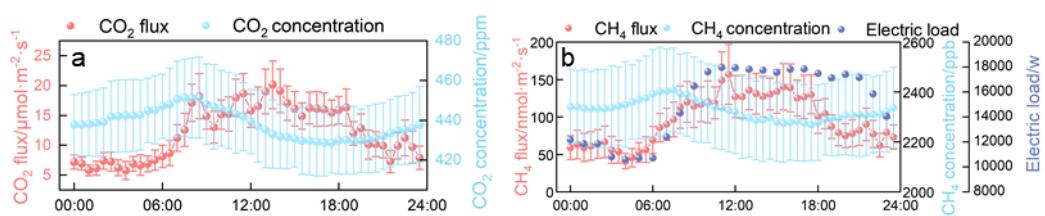
219 Figure 1 Daily variations in the CO_2 and CH_4 concentrations, fluxes, and electricity loads

221 Figure 1 Daily variations in the CO_2 and CH_4 concentrations, fluxes, and electricity loads

222 **3.2 Homology between CO_2 and CH_4**

223 The CO_2 and CH_4 fluxes showed a significant correlation along all directions (Figure 2), with

224 correlation coefficients greater than that at the center of Loz, Poland (0.50)(Pawlak et al., 2016), but

225 the low correlation between the CO_2 and CH_4 fluxes and the temperature excludes the conclusion

226 that biological sources dominate their emissions (Figure S8). Therefore, CO_2 and CH_4 share the

227 same anthropogenic sources within the source area. This homology is also reflected in their spatial

228 distributions, with high fluxes distributed mainly south of the tower, which is more densely

229 populated and encompasses complex industrial structures, and much lower fluxes in the northern

230 forest and park areas (Figure 3a, b). The correlation between the spatial distributions of the CO_2 and

231 CH_4 fluxes reached 0.98, demonstrating the common impact of similar anthropogenic sources on

232 their emissions. The linear fitting results at 150° and 240° indicated the highest correlation

233 coefficient (0.82) along all directions (Figure 2), further supporting this viewpoint.

234
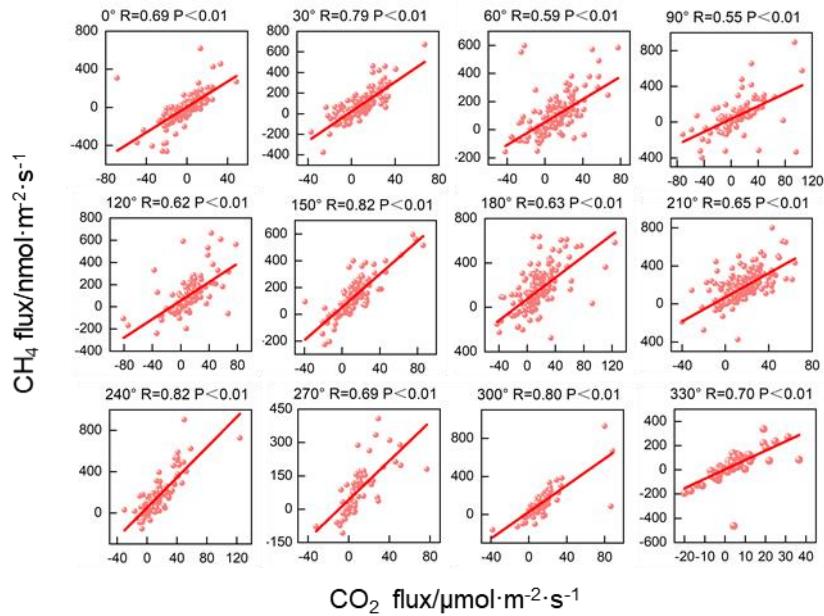
Figure 2 Linear fitting results for the 30-minute CH_4 and CO_2 fluxes in the 12 directions

236
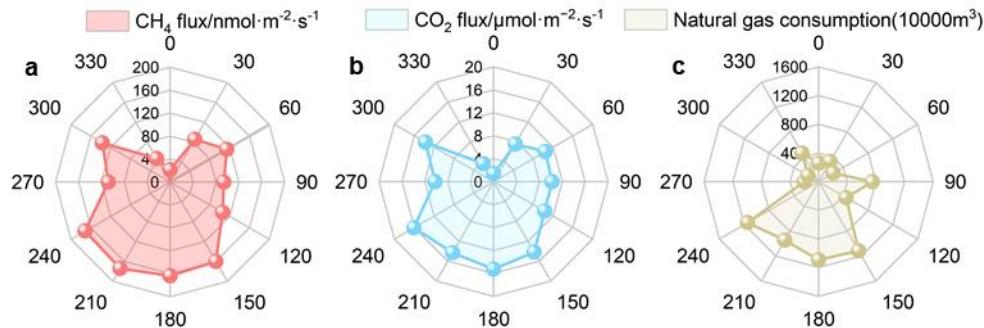
Figure 3 Mean CH_4 and CO_2 concentrations, fluxes and natural gas consumption in the 12

directions

4. DISCUSSION

4.1 Driver of the homology between CO_2 and CH_4

After the introduction of natural gas in 1985, the proportion of natural gas in the fossil fuel industry of Beijing increased annually, especially when coal was replaced with natural gas and electricity in 2014 and 2018, respectively, and natural gas became the most consumed fossil fuel (Figure 4a). According to the 2022 Beijing Statistical Yearbook (https://nj.tjj.beijing.gov.cn/nj/main/2023-tjnj/zk/e/indexch.htm), natural gas is used mainly for thermal power generation and heating (accounting for 69%). Owing to the low proportion of heating in summer, natural gas in Beijing is mostly used for thermal power generation in summer. Owing to

249 the difficulty in obtaining hourly electricity generation data, we obtained a daily variation curve of

250 the electricity load in Beijing based on the statistical data (power plants usually calculate the

251 required electricity generation based on the electricity load) (https://www.gov.cn/xinwen/2019-

252 12/30/5465088/files/e3682ce168c8427b886a43a790d66c2c.pdf) (Figure 1b). The daily variation in

253 the electricity load is highly consistent with that in the CH_4 flux, with the maximum CH_4 flux

254 occurring at 11:00 pm during the peak electricity consumption period. After 16:00 pm, the electricity

255 load and CH_4 flux decrease synchronously. Thus, the daily variation in the CH_4 flux is driven by

256 natural gas consumption. We gridded the natural gas consumption data (Figure S9) and calculated

257 the mean natural gas consumption along all directions within the flux source area (Figure 3c).

258 Notably, a high consistency between the spatial distributions of the CO_2 and CH_4 fluxes and natural

259 gas consumption was found, which reflects that after the adjustment of the energy structure in

260 Beijing, natural gas became the main source of CO_2 and CH_4. Considering the high photosynthetic

261 absorption of CO_2 by plants in summer, this conclusion also applies to the other seasons, which

262 supports the hypothesis that natural gas is the main source of winter CO_2 emissions in Beijing, as

263 determined based on the isotope tracing method(Wang et al., 2022; Wang et al., 2022).

264 To verify this conclusion and identify the primary phases of natural gas leakage, we conducted

265 mobile observations during winter and summer around large petrochemical plants, gas storage tanks,

266 and power plants in Beijing. Given real-time variations in gas concentrations influenced by

267 meteorological conditions and pollution transport, it was essential to determine background

268 concentrations at each time point. The current mainstream approach for determining background

269 values involves calculating the 5th or 10th percentile within a sliding window of 5 minutes (±2.5 min)

270 or 10 minutes (±5 min) centered on the target timestamp (Pu et al., 2023, Well et al., 2018; Well et

271 al., 2019). We compared and evaluated the results applying different combinations of time windows

272 or percentile following the method of Schiferl et al., (2025). (Text. S3). The 10-min time window

273 with 5th percentile was used here to calculate the background value. The enhancement concentration

274 can be defined as the difference between the observed value and the background value at the

275 corresponding time. There was significant CH_4 leakage around the gas storage tanks and power

276 plants in both winter and summer. Notably, the observed CH_4 hotspots were located in the downzone

277 of potential leakage sources; therefore, we attribute the high CH_4 concentration to the emissions of

278 these potential natural gas leakage sources. In winter, hotspots with concentrations higher than the

279   background value of 1759 ppb appeared around the gas storage tank (Figure 5a), corresponding to

280   an enhancement concentration of CH_4 (E-CH_4) and enhancement concentration of CO_2 (E-CO_2)

281   fingerprint line with a slope of 0.11 (Figure 6a). In addition, the enhancement concentration

282   fingerprint slopes of the other hotspot zones were 0.06 and 0.07, respectively, indicating varying

283   degrees of leakage around the gas storage tank(Sun et al., 2019).The enhancement concentration

284   fingerprint in summer also revealed leakage related to gas storage equipment (Figure 5b), with a

285   slope of 0.04, analogous to that of 0.06 in winter. Similar to gas storage tanks, natural gas leakage

286   hotspots have been observed in various equipment in power plants. For example, fingerprints with

287   a slope of 0.005 (Figure 6d) in summer reflected leakage related to combustion devices or pipeline

288   in power plants(Lamb et al., 1995), whereas fingerprints with a slope of 0.015, 0.02 or 0.05 reflected

289   leakage related to storage facilities (Figure 6c,d)(Hurry et al., 2016). We also discovered natural gas

290   leakage near the petrochemical plant (Figure 6e), the line with a slope of 0.02 was related to the gas

291   storage equipment, and the line with a slope of 0.005 was relevant to the natural gas combustion

292   equipment. As important sources of methane, landfills have received widespread attention, so we

293   also conducted mobile observations near a large landfill outside the Fifth Ring Road in Beijing,

294   which was a hotspot exhibiting a level exceeding the minimum concentration of 1375 ppb (Figure

295   5f). The concentration fingerprints were relatively disordered and significantly differed from those

296   of CH_4 emissions dominated by natural gas (Figure 6f), indicating that waste disposal processes are

297   relatively complex and cannot be ignored in cities(Cusworth et al., 2024).

298   Converting observed concentration increments into emission rates is a simple means of

299   quantifying natural gas leakage, which is subject to atmospheric conditions and potential leak source

300   locations. Weller et al., (2018; 2019) developed a model based on the relationship between the

301   enhancement concentration and emission rate. The specific formula is shown in Text S4. The model

302   assumes that CH_4 enhancement is the best predictor of the leakage emission rate and that a greater

303   leakage emission rate corresponds to greater CH_4 enhancement. The method sets a minimum

304   threshold for the observed CH_4 concentration, which is 110% of the background value, to filter out

305   concentration changes caused by measurement. Moreover, when multiple detections are conducted

306   for the same leakage source, it is necessary to average the CH_4 enhancement values and then

307   substitute them into the above formula. We estimated the natural gas leakage emission rates from

308   different leakage sources with this method, and the confidence interval (CI) based on the Bootstrap

309 method was used to estimate the uncertainty of the leakage rate. The natural gas leakage rate from

310 the gas storage tank and power plant in winter were 7.4 ± 0.1 g/min and 0.6 ± 0.03 g/min,

311 respectively, and the natural gas leakage rate from the gas storage tank and power plant in summer

312 were 1.2 ± 0.04 g/min and 2.1 ± 0.07 g/min, respectively. The natural gas leakage rate near the

313 petrochemical plant was 0.6 ± 0.04 g/min, which was lower than the results of Ars et al., (2020) on

314 the leakage rates of Toronto's natural gas distribution network (3.52–10.56 g/min), but they noted

315 that Well's method underestimated the leakage rate because it ignored smaller concentration

316 enhancements. A significant uncertainty in this method lies in the distance between the leakage point

317 and the vehicle; unfortunately, determining the distance between the two points in practical

318 operation is difficult, which may confound the estimation of methane leakage. Therefore, sufficient

319 mobile experiments should be conducted in subsequent work to accurately calculate natural gas

320 leakage in Beijing.

321

322
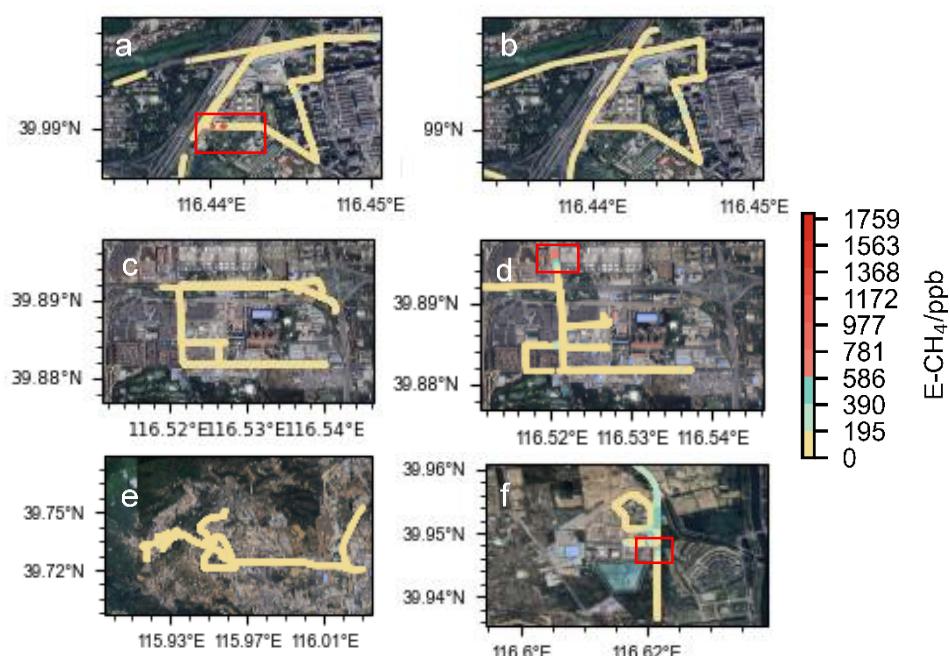
323 Figure 5 CH$_4$ enhancement concentration distribution map based on vehicle observations (a, c

324 show storage tanks and thermal power plants in winter; b, d show storage tanks and thermal power

325 plants in summer; e shows petrochemical plants; f shows waste disposal station; and the red box

326   represents high leakage value)
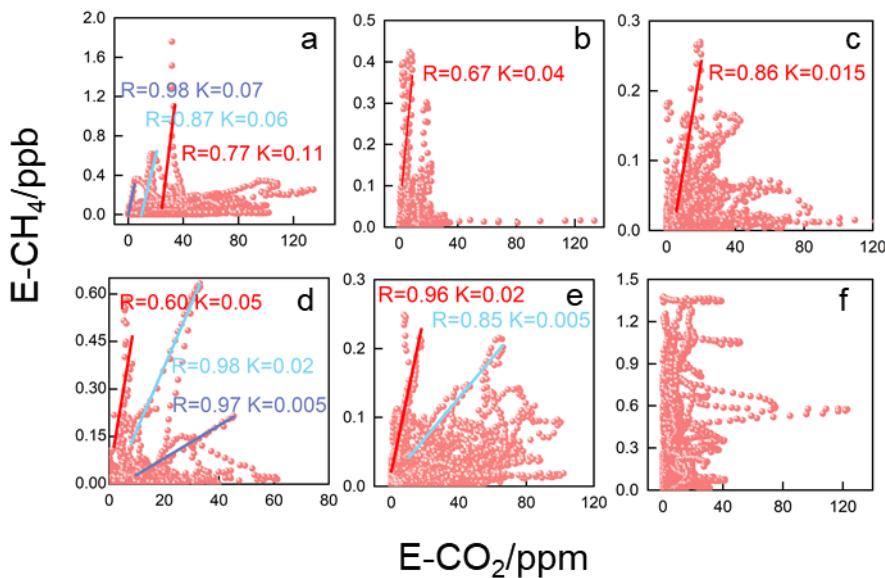
Figure 6 Fitting of the CO$_2$ and CH$_4$ concentration enhancement values (a, c show the fitting results for the gas storage tanks and power plants in winter; b, d show the fitting results for the gas storage tanks and power plants in summer; e shows the petrochemical plants; and f shows the waste disposal stations. Different fitting lines represent various leakage sources.)

4.2 Climatic effects of natural gas (NG) losses and their impact on carbon neutrality

Based on the natural gas consumption and flux data for the flux source area, the estimated upper limit of the natural gas leakage rate in Beijing reached 1.12 % ±0.22 % (Text. S5), and the lower limit of natural gas leakage in Beijing was estimated to be 0.82 % considering the emissions from biogenic sources (Text. S6). If the CH$_4$ fluxes were attributable solely to pipeline leakage processes, the CH$_4$ fluxes should remain relatively stable throughout the day without significant diurnal variations, given the constant pressure in urban pipeline pressures. However in our observations, the CH$_4$ fluxes exhibited pronounced diurnal patterns and their spatial distribution positively correlated with natural gas consumption. This indicates that CH$_4$ emissions in Beijing originate predominantly from consumption-oriented leakage processes. Consequently, as natural gas consumption surges during winter heating periods, CH$_4$ emissions from these processes (e.g., fugitive emissions from electrical devices) also increase. As a result, the ratio of emissions to consumption (leakage rate) remains relatively stable. Thus, the CH$_4$ leakage rate measured in summer is representative of year-round leakage rate of natural gas.

Our measured leakage rate was lower than the value of 2.07 % calculated based on the purchase

348 and sales statistics and the statistical mean value of 1.1 %–1.65 % reported by the American

349 Petroleum Institute (https://www.api.org/). Nevertheless, the contributions of CH_4 to climate

350 warming are 8.37 % and 23.17 % of those of CO_2 at the 100- and 20-year scales, respectively,

351 according to the determined CO_2 and CH_4 fluxes and the GWP of methane. With the arrival of the

352 winter heating season, climate forcing will further increase on a yearly scale. Assuming that the

353 natural gas consumption in Beijing during the heating season is 5 times greater than that during the

354 other seasons (according to Beijing Gas in 2019), that oil consumption does not significantly

355 fluctuate throughout the year and that both the CO_2 and CH_4 fluxes are positively correlated with

356 fossil fuel consumption and natural gas leakage, the climate forcing effect of natural gas leakage in

357 2022 was 11.47 % on a 100-year scale and could reach as high as 31.56 % on a 20-year scale.

358 However, when the same amount of heat is generated, the use of natural gas could yield CO_2

359 emission reductions of 50 % relative to coal and of only approximately 30 % relative to oil.

360 Therefore, the reduction in greenhouse gas emissions resulting from natural gas combustion

361 compared with that resulting from the combustion of other fossil fuels may be offset by the climate

362 forcing effect of CH_4 leakage in the short term, making it difficult for natural gas to become a

363 transitional energy source for energy transition.

364 To assess the impact of natural gas leakage on carbon peak and carbon neutrality based on our

365 quantified leakage rate, scaling the Beijing-derived leakage rate to a national level is needed.

366 However, due to the absence of leakage rate data from other cities, we can provide only a rough

367 estimate based on available data as follows: according to the 14th Five-Year Plan for National Urban

368 Infrastructure Development (https://www.gov.cn/zhengce/zhengceku/2022-

369 07/31/5703690/files/d4ebd608827e41138701d06fe6133cdb.pdf), cities in China are divided into

370 three categories—major cities (natural gas penetration rate ≥85 %), medium cities (natural gas

371 penetration rate ≥75 %), and small cities (natural gas penetration rate ≥60 %). The China Gas

372 Development Report 2023 further supplements pipeline coverage

373 progress(https://www.emerinfo.cn/download/zgtrqfzbg2003001.pdf), indicating that large cities

374 and developed regions (e.g., Beijing, the Yangtze River Delta, the Pearl River Delta) accounted for

375 approximately 30 %–40 % of the national pipeline length in 2022, here set at 35 %. Small/medium

376 cities constituted 60 %–70 % of the total pipeline length, here set at 65 %. A study based on Bayesian

377 network modeling revealed that leakage probabilities in small/medium cities are 1.8 times higher

378 than those in major cities (95% CI: 1.6–2.0)(Gao et al., 2024). Consequently, the national leakage

379 rate was calculated as 1.7 % (95 % CI: 1.57 %–1.85 %)=0.35×1.12 %+0.65×1.12 %×1.8(95 %

380 CI:1.6–2.0).

381   Then we adopted the results of the Global Climate Governance Strategy and China's Carbon

382 Neutrality Path Outlook(Wang et al., 2021), which indicates that CO_2 emissions in China under the

383 carbon neutrality scenario reach approximately 2.1 Gt. We calculated CH_4 leakage in the

384 corresponding year based on the natural gas consumption level under the future scenario of the

385 China Energy Outlook 2060 (SINOPEC 2021)(Economics-and-Development-Research-Institute,

386 2021). All of the calculation results were converted CO_2 equivalents (CO_2e) according to the GWP

387 on a 20-year scale (Figure 4b). After taking into account the natural gas leakage process, the CO_2e

388 in China will still peak by 2030. However, the CO_2e resulting from natural gas leakage will reach

389 0.37 Gt (95 % CI: 0.34 Gt–0.40 Gt) in 2060, compared to 0.26 Gt previously. This accounts for

390 approximately 16.6 % (95 % CI: 15.4 %–17.9 %) of the total CO_2 emissions (excluding natural gas

391 leakage) and 35.9 % (95 % CI: 33.2 %–38.8 %) of the total CO_2 emissions from natural gas

392 combustion, which is comparable to the CO_2 emissions from coal combustion (0.35 Gt). Since

393 natural carbon sinks do not show significant short-term fluctuations, the future increase in carbon

394 sinks will mainly rely on carbon capture and storage (CCS) technology. Given the current estimated

395 CO_2 capture rate of CCS technology (0.1 Gt/year, as estimated by the China Energy Outlook 2060

396 (SINOPEC 2021)), the achievement of carbon neutrality in China will likely be delayed by nearly

397 three to four years. Therefore, when determining future natural gas consumption levels, it is

398 necessary to both consider the leakage effects of natural gas and utilize carbon modeling.
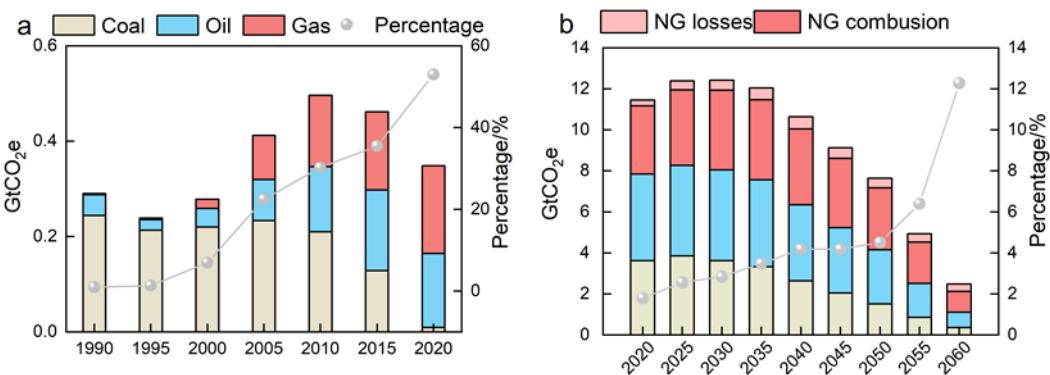
399

400 Figure 4 Terminal consumption of coal, oil, and natural gas and their proportions from 1990 to
401   2020(a) Since diesel-powered trucks are allowed only at night on the Fifth Ring Road and
402 kerosene, which is used mainly in aviation and is not included in the flux source area, oil mainly

comprises gasoline in this case), CO_2 equivalent from coal, oil and natural gas (losses and combustion) in the future scenario (estimated by China Energy Outlook 2060 released by SINOPEC in 2021), and CO_2 equivalent of natural gas leakage as a proportion of natural gas (NG) combustion emissions(b)

4.3 Policy implications

Our observations revealed a strong correlation between CH_4 emissions and natural gas consumption in terms of both their daily variations and spatial distributions, that is to say, the terminal consumption process drive natural gas leakage in Beijing. Liu et al., (2023) established a bottom-up emission inventory and reported that the terminal use process in Beijing accounts for 80% of the total methane emissions in the entire natural gas supply chain. Therefore, the Chinese government may need to expand the detection of pipeline leakage to the entire natural gas industry chain.

Notably, existing grid-based inventory products also exhibit significant uncertainty in terms of methane sources. The extracted inventory originates from the Emissions Database for Global Atmospheric Research (EDGAR) (https://edgar.jrc.ec.europa.eu/EDGARv8.0). Although the mean methane flux (126.34 $nmol \cdot m^{-2} \cdot s^{-1}$) within the source area is close to our results, the terminal use process accounts for only approximately 13 % of the annual methane emissions, suggesting that many potential urban methane sources could have been missed, which should be considered in inventory refinement in the future.

In addition, minimizing the methane leakage rate could ensure the early realization of carbon neutrality in China. Although methane emission control has been included in the agenda for the first time in the Methane Emission Control Action Plan promulgated in 2023, which clearly highlights the need to promote the application of leak detection and repair technology and to enhance the comprehensive recovery and utilization of methane, methane leakage standards have not been updated. Previous methane leakage standards focused only on controlling the amount of methane leakage from a safe perspective, thereby ignoring the climate effects of natural gas leakage. China must urgently develop a strict and detailed set of natural gas leakage standards.

5. SUMMARY AND CONCLUSIONS

This study utilized the eddy covariance method to measure CO_2 and CH_4 fluxes at 220-m height in urban Beijing, providing critical insights into surface-atmosphere exchanges of greenhouse gases

in the region. First, urban areas unequivocally act as net sources of both CO_2 and CH_4. The daily mean fluxes were 12.21 ± 1.75 $\mu mol \cdot m^{-2} \cdot s^{-1}$ for CO_2 and 95.54 ± 18.92 $nmol \cdot m^{-2} \cdot s^{-1}$ for CH_4, with daytime emissions significantly exceeding nighttime levels, highlighting the importance of anthropogenic influences.

Although diurnal variation patterns differed slightly between CO_2 and CH_4 fluxes, their strong correlation indicates shared dominant sources. Spatial distribution analysis revealed high consistency between both fluxes and natural gas consumption patterns, confirming natural gas as a common source. With Beijing's energy restructuring, natural gas has become the dominated terminal energy consumption. Its combustion releases substantial CO_2, while leakage processes emit CH_4, as validated by mobile observations detecting CH_4 fugitive emissions during production, storage and use stages. Although biogenic sources could contribute to CH_4 emissions, they account for at most 27 % of total CH_4 fluxes in the source area, ruling out the view that biological sources dominate both emissions. Attributing all CH_4 emissions to natural gas usage, the upper leakage rate of natural gas in Beijing was calculated as $1.12\ \%\pm0.22\ \%$.

The CH_4 emissions from natural gas will exacerbate climate warming. Calculated flux results showed that the contribution of CH_4 to climate warming on a century and 20-year scale can reach as high as 8.37 % and 23.17 % of CO_2, respectively. On the basis of predicted energy report and calculated leakage rate, it is predicted that natural gas leakage will delay China's realization of carbon neutrality, which necessitates urgent attention to mitigate associated climate effects.

SUPPORTING INFORMATION

Details about the Beijing Meteorological Tower, eddy observation system and navigation observation station, daily summer variation in CO_2 flux from 2009 to 2017, total consumption, electricity inflow and the proportion of natural gas in total energy consumption from 2013-2022, spatial distribution of CO_2 and CH_4 fluxes with wind speed and direction, grid distribution of natural gas consumption in Beijing, calculation methods of the flux source area and natural gas leakage rate, uncertainty analysis of flux calculation, estimation of non-natural gas sources

ACKNOWLEDGMENTS

This work was supported by the National Key R&D Program of China (2023YFC3706103), the Strategic Priority Research Program of the Chinese Academy of Sciences (XDB0760200), the Beijing Municipal Natural Science Foundation (No. 8222075), the Youth Cross Team Scientific

464 Research Project of the Chinese Academy of Sciences (No. JCTD-2021-10) and the S&T Program
465 of Hebei (22373903D).

466 **DATA AVAILABILITY**

467 All the data generated or analyzed in this study are included in the published article and are available

468 from the authors upon reasonable request.

469 **COMPETING INTERESTS**

470 The authors declare that they have no competing interests.

471 **REFERENCES**

472 Ars, S., Vogel, F., Arrowsmith, C., Heerah, S., Knuckey, E., Lavoie, J., Lee, C., Pak, N. M., Phillips,
473   J. L., and Wunch, D.: Investigation of the Spatial Distribution of Methane Sources in the
474   Greater Toronto Area Using Mobile Gas Monitoring Systems, Environ. Sci. Technol., 54,
475   15671-15679, http://doi.org/10.1021/acs.est.0c05386, 2020.
476 Barlow, J. F.: Progress in observing and modelling the urban boundary layer, Urban Climate, 10,
477   216-240, http://doi.org/10.1016/j.uclim.2014.03.011, 2014.
478 Chen, Z., Jacob, D. J., Nesser, H., Sulprizio, M. P., Lorente, A., Varon, D. J., Lu, X., Shen, L., Qu,
479   Z., Penn, E., and Yu, X.: Methane emissions from China: a high-resolution inversion of
480   TROPOMI satellite observations, Atmos. Chem. Phys., 22, 10809-10826,
481   http://doi.org/10.5194/acp-22-10809-2022, 2022.
482 Cheng, X. L., Liu, X. M., Liu, Y. J., and Hu, F.: Characteristics of CO_2 concentration and flux in the
483   Beijing urban area, J. Geophys. Res-Atmos., 123, 1785-1801,
484   http://doi.org/10.1002/2017JD027409, 2018.
485 Cusworth, D. H., Duren, R. M., Ayasse, A. K., Jiorle, R., Howell, K., Aubrey, A., Green, R. O.,
486   Eastwood, M. L., Chapman, J. W., Thorpe, A. K., Heckler, J., Asner, G. P., Smith, M. L., Thoma,
487   E., Krause, M. J., Heins, D., and Thorneloe, S.: Quantifying methane emissions from United
488   States landfills, Science, 383, 1499-1504, http://doi.org/10.1126/science.adi7735, 2024.
489 Cusworth, D. H., Jacob, D. J., Sheng, J.-X., Benmergui, J., Turner, A. J., Brandman, J., White, L.,
490   and Randles, C. A.: Detecting high-emitting methane sources in oil/gas fields using satellite
491   observations, Atmos. Chem. Phys., 18, 16885-16896, http://doi.org/10.5194/acp-18-16885-
492   2018, 2018.
493 Donateo, A., Conte, M., Grasso, F. M., and Contini, D.: Seasonal and diurnal behaviour of size
494   segregated particles fluxes in a suburban area, Atmos. Environ, 219, 117052,
495   http://doi.org/10.1016/j.atmosenv.2019.117052, 2019.
496 Duren, R. M., Thorpe, A. K., Foster, K. T., Rafiq, T., Hopkins, F. M., Yadav, V., Bue, B. D.,
497   Thompson, D. R., Conley, S., Colombi, N. K., Frankenberg, C., McCubbin, I. B., Eastwood,
498   M. L., Falk, M., Herner, J. D., Croes, B. E., Green, R. O., and Miller, C. E.: California's methane
499   super-emitters, Nature, 575, 180-184, http://doi.org/10.1038/s41586-019-1720-3, 2019.
500 Economics-and-Development-Research-Institute: World and China Energy Outlook 2060,
501   https://www.docin.com/p-2955292161.html, 2021.
502 Environmental-Protection-Agency: Understanding global warming potentials,
503   https://www.epa.gov/ghgemissions/understandingglobal-warming-potentials, last accessed: 22

Oct. 2024.

Fan, S. M., Wofsy, S. C., Bakwin, P. S., Jacob, D. J., and Fitzjarrald, D. R.: Atmosphere−biosphere exchange of CO_2 and O_3 in the central Amazon Forest, JGR: Atmospheres, 95, 16851-16864, http://doi.org/10.1029/JD095iD10p16851, 2012.

Frankenberg, C., Thorpe, A. K., Thompson, D. R., Hulley, G., Kort, E. A., Vance, N., Borchardt, J., Krings, T., Gerilowski, K., Sweeney, C., Conley, S., Bue, B. D., Aubrey, A. D., Hook, S., and Green, R. O.: Airborne methane remote measurements reveal heavy-tail flux distribution in Four Corners region, Proc. Natl. Acad. Sci. U. S. A., 113, 9734-9739, http://doi.org/10.1073/pnas.1605617113, 2016.

Gao, S., Tian, W., and Wang, C.: A method, system, equipment, and medium for determining methane leakage in a natural gas pipeline network: 202410249186, in Chinese, 2024.

Gioli, B., Toscano, P., Lugato, E., Matese, A., Miglietta, F., Zaldei, A., and Vaccari, F. P.: Methane and carbon dioxide fluxes and source partitioning in urban areas: the case study of Florence, Italy, Environ Pollut, 164, 125-131, http://doi.org/10.1016/j.envpol.2012.01.019, 2012.

Helfter, C., Tremper, A. H., Halios, C. H., Kotthaus, S., Bjorkegren, A., Grimmond, C. S. B., Barlow, J. F., and Nemitz, E.: Spatial and temporal variability of urban fluxes of methane, carbon monoxide and carbon dioxide above London, UK, Atmos. Chem. Phys., 16, 10543-10557, http://doi.org/10.5194/acp-16-10543-2016, 2016.

Hurry, J., Risk, D., Lavoie, M., Brooks, B.-G., Phillips, C. L., and Göckede, M.: Atmospheric monitoring and detection of fugitive emissions for Enhanced Oil Recovery, Int. J. Greenh. Gas Con., 45, 1-8, http://doi.org/10.1016/j.ijggc.2015.11.031, 2016.

Kaimal, J. C., and Finnigan, J. J.: Atmospheric boundary layer flows: their structure and measurement. New York: Oxford University Press, 1994.

Kaimal, J. C., Wyngaard, J. C., Izumi, Y., and Coté, O. R.: Spectral characteristics of surface−layer turbulence, Quart. J. R. Met. Soc., 98, 563-589, http://doi.org/10.1002/qj.49709841707, 1972.

Kemfert, C., Präger, F., Braunger, I., Hoffart, F. M., and Brauers, H.: The expansion of natural gas infrastructure puts energy transitions at risk, Nature Energy, 7, 582-587, http://doi.org/10.1038/s41560-022-01060-3, 2022.

Kljun, N., Calanca, P., Rotach, M. W., and Schmid, H. P.: A Simple Parameterisation for Flux Footprint Predictions, Boundary-Layer Meteorology, 112, 503-523, http://doi.org/10.1023/b:Boun.0000030653.71031.96, 2004.

Lamb, B. K., McManus, J. B., Shorter, J. H., Kolb, C. E., Mosher, B., Harriss, R. C., Allwine, E., Blaha, D., Howard, T., Guenther, A., Lott, R. A., Siverson, R., Westburg, H., and Zimmerman, P.: Development of atmospheric tracer methods to measure methane emissions from natural gas facilities and urban areas, Environ. Sci. Technol., 29, 1468-1479, http://doi.org/10.1021/es00006a007, 1995.

Lee, X.: Handbook of micrometeorology: A Guide for surface Flux Measurement and Analysis. New York: Klewer Academic Publishers, 2004.

Liu, H. Z., Feng, J. W., Järvi, L., and Vesala, T.: Four-year (2006–2009) eddy covariance measurements of CO_2 flux over an urban area in Beijing, Atmos. Chem. Phys., 12, 7881-7892, http://doi.org/10.5194/acp-12-7881-2012, 2012.

Liu, S., Liu, K., Wang, K., Chen, X., and Wu, K.: Fossil-Fuel and Food Systems Equally Dominate Anthropogenic Methane Emissions in China, Environ. Sci. Technol., 57, 2495-2505,

547   http://doi.org/10.1021/acs.est.2c07933, 2023.

548   Liu, Z., Liu, Z., Song, T., Gao, W., Wang, Y., Wang, L., Hu, B., Xin, J., and Wang, Y.: Long-term
549   variation in CO_2 emissions with implications for the interannual trend in PM(2.5) over the last
550   decade   in   Beijing,   China,   Environ.   Pollut.,   266,   115014,
551   http://doi.org/10.1016/j.envpol.2020.115014, 2020.

552   Mauder, M., and Foken, T.: Documentation and Instruction Manual of the Eddy Covariance
553   Software Package TK2, Proc. R. Soc. Med., 26, 42-46, http://doi.org/10.5281/zenodo.20349,
554   2004.

555   Moncrieff, J. B., Malhi, Y., and Leuning, R.: The propagation of errors in long‑term measurements
556   of land‑atmosphere fluxes of carbon and water, Global Change Biology, 2, 231-240,
557   http://doi.org/10.1111/j.1365-2486.1996.tb00075.x, 1996.

558   Pawlak, W., and Fortuniak, K.: Eddy covariance measurements of the net turbulent methane flux in
559   the city centre – results of 2-year campaign in Łódź, Poland, Atmos. Chem. Phys., 16, 8281-
560   8294, http://doi.org/10.5194/acp-16-8281-2016, 2016.

561   Pu, W., Sheng, J., Tian, P., Huang, M., Liu, X., Collett Jr, J.L., Li, Z., Zhao, X., He, D., Dong, F.:
562   On-road mobile mapping of spatial variations and source contributions of ammonia in Beijing,
563   China, Sci. Total Environ., 864, 160869, 2023.

564   Sargent, M. R., Floerchinger, C., McKain, K., Budney, J., Gottlieb, E. W., Hutyra, L. R., Rudek, J.,
565   and Wofsy, S. C.: Majority of US urban natural gas emissions unaccounted for in inventories,
566   Proc. Natl. Acad. Sci. U. S. A., 118, e2105804118, http://doi.org/10.1073/pnas.2105804118,
567   2021.

568   Schiferl, L.D., Hallward-Driemeier, A., Zhao, Y., Toledo-Crow, R., and Commane, R.: Missing
569   wintertime methane emissions from New York City related to combustion, EGUsphere, 2025,
570   1-28, https://doi.org/10.5194/egusphere-2025-345, 2025.

571   Seneviratne, S. I., Rogelj, J., Seferian, R., Wartenburger, R., Allen, M. R., Cain, M., Millar, R. J.,
572   Ebi, K. L., Ellis, N., Hoegh-Guldberg, O., Payne, A. J., Schleussner, C. F., Tschakert, P., and
573   Warren, R. F.: The many possible climates from the Paris Agreement's aim of 1.5 degrees C
574   warming, Nature, 558, 41-49, http://doi.org/10.1038/s41586-018-0181-4, 2018.

575   Shen, L., Jacob, D. J., Gautam, R., Omara, M., Scarpelli, T. R., Lorente, A., Zavala-Araiza, D., Lu,
576   X., Chen, Z., and Lin, J.: National quantifications of methane emissions from fuel exploitation
577   using high resolution inversions of satellite observations, Nat. Commun., 14, 4948,
578   http://doi.org/10.1038/s41467-023-40671-6, 2023.

579   Sherwin, E. D., Rutherford, J. S., Zhang, Z., Chen, Y., Wetherley, E. B., Yakovlev, P. V., Berman, E.
580   S. F., Jones, B. B., Cusworth, D. H., Thorpe, A. K., Ayasse, A. K., Duren, R. M., and Brandt,
581   A. R.: US oil and gas system emissions from nearly one million aerial site measurements,
582   Nature, 627, 328-334, http://doi.org/10.1038/s41586-024-07117-5, 2024.

583   Sun, W., Deng, L., Wu, G., Wu, L., Han, P., Miao, Y., and Yao, B.: Atmospheric Monitoring of
584   Methane   in   Beijing   Using   a   Mobile   Observatory,   Atmosphere,   10,   554,
585   http://doi.org/10.3390/atmos10090554, 2019.

586   Vickers, D., and Mahrt, L.: Quality Control and Flux Sampling Problems for Tower and Aircraft
587   Data,   J.   Atmos.   Oceanic   Technol.,   14,   512-526,   http://doi.org/10.1175/1520-
588   0426(1997)014<0512:Qcafsp>2.0.Co;2, 1997.

589   Wang, P., Zhou, W., Xiong, X., Wu, S., Niu, Z., Cheng, P., Du, H., and Hou, Y.: Stable carbon
590   isotopic characteristics of fossil fuels in China, Sci. Total. Environ., 805, 150240,

591   http://doi.org/10.1016/j.scitotenv.2021.150240, 2022.

592   Wang, P., Zhou, W., Xiong, X., Wu, S., Niu, Z., Yu, Y., Liu, J., Feng, T., Cheng, P., Du, H., Lu, X.,
593   Chen, N., and Hou, Y.: Source Attribution of Atmospheric CO_2 Using ^{14}C and ^{13}C as Tracers
594   in Two Chinese Megacities During Winter, JGR: Atmospheres, 127, e2022JD036504,
595   http://doi.org/10.1029/2022jd036504, 2022.

596   Wang, Y., Guo, C. H., Chen, X. J., Jia, L. Q., Guo, X. N., Chen, R. S., and Wang, H. D.: Global
597   climate governance strategies and prospects for China's carbon neutrality path. Forecasting
598   And Prospects Research Report, 2021.

599   Webb, E. K., Pearman, G. I., and Leuning, R.: Correction of flux measurements for density effects
600   due to heat and water vapour transfer, Q. J. R. Meteorolog. Soc., 106, 85-100,
601   http://doi.org/10.1002/qj.49710644707, 2007.

602   Weller, Z. D., Roscioli, J. R., Daube, W. C., Lamb, B. K., Ferrara, T. W., Brewer, P. E., and von
603   Fischer, J. C.: Vehicle-Based Methane Surveys for Finding Natural Gas Leaks and Estimating
604   Their Size: Validation and Uncertainty, Environ. Sci. Technol., 52, 11922-11930,
605   http://doi.org/10.1021/acs.est.8b03135, 2018.

606   Weller, Z. D., Yang, D. K., and von Fischer, J. C.: An open source algorithm to detect natural gas
607   leaks from mobile methane survey data, PLoS One, 14, e0212287,
608   http://doi.org/10.1371/journal.pone.0212287, 2019.

609   Wunch, D., Toon, G. C., Hedelius, J. K., Vizenor, N., Roehl, C. M., Saad, K. M., Blavier, J.-F. L.,
610   Blake, D. R., and Wennberg, P. O.: Quantifying the loss of processed natural gas within
611   California's South Coast Air Basin using long-term measurements of ethane and methane,
612   Atmos. Chem. Phys., 16, 14091-14105, http://doi.org/10.5194/acp-16-14091-2016, 2016.

613   Zöll, U., Brümmer, C., Schrader, F., Ammann, C., Ibrom, A., Flechard, C. R., Nelson, D. D.,
614   Zahniser, M., and Kutsch, W. L.: Surface–atmosphere exchange of ammonia over peatland
615   using QCL-based eddy-covariance measurements and inferential modeling, Atmos. Chem.
616   Phys., 16, 11283-11299, http://doi.org/10.5194/acp-16-11283-2016, 2016.

617